How to cite: *Angew. Chem. Int. Ed.* **2023,** *62,* e202302490
doi.org/10.1002/anie.202302490

Lanthipeptides

Discovery of the Lanthipeptide Curvocidin and Structural Insights into its Trifunctional Synthetase CuvL

*Arnar Sigurdsson, Berta M. Martins, Simon A. Düttmann, Martin Jasyk, Benjamin Dimos-Röhl, Felix Schöpf, Manuel Gemander, Caroline H. Knittel, Romina Schnegotzki, Bianca Schmid, Simone Kosol, Lea Pommerening, María Gonzáles-Viegaz, Maria Seidel, Manuela Hügelland, Silke Leimkühler, Holger Dobbek, Andi Mainz, and Roderich D. Süssmuth**

Abstract: Lanthipeptides are ribosomally-synthesized natural products from bacteria featuring stable thioether-crosslinks and various bioactivities. Herein, we report on a new clade of tricyclic class-IV lanthipeptides with curvocidin from *Thermomonospora curvata* as its first representative. We obtained crystal structures of the corresponding lanthipeptide synthetase CuvL that showed a circular arrangement of its kinase, lyase and cyclase domains, forming a central reaction chamber for the iterative substrate processing involving nine catalytic steps. The combination of experimental data and artificial intelligence-based structural models identified the N-terminal subdomain of the kinase domain as the primary site of substrate recruitment. The ribosomal precursor peptide of curvocidin employs an amphipathic α-helix in its leader region as an anchor to CuvL, while its substrate core shuttles within the central reaction chamber. Our study thus reveals general principles of domain organization and substrate recruitment of class-IV and class-III lanthipeptide synthetases.

[*] A. Sigurdsson, Dr. S. A. Düttmann, M. Jasyk, B. Dimos-Röhl, F. Schöpf, M. Gemander, Dr. C. H. Knittel, Dr. R. Schnegotzki, B. Schmid, Dr. S. Kosol, L. Pommerening, M. Seidel, M. Hügelland, Dr. A. Mainz, Prof. Dr. R. D. Süssmuth
Fakultät II–Institut für Chemie, Technische Universität Berlin
Straße des 17. Juni 124, 10623 Berlin (Germany)
E-mail: roderich.suessmuth@tu-berlin.de
Homepage: https://www.tu.berlin/biochemie

Dr. B. M. Martins, M. Gonzáles-Viegaz, Prof. Dr. H. Dobbek
Institut für Biologie–Strukturbiologie/Biochemie, Humboldt Universität zu Berlin
Philippstraße 13, 10115 Berlin (Germany)

Prof. Dr. S. Leimkühler
Institut für Biochemie und Biologie, Universität Potsdam
Karl-Liebknecht-Str. 24–25, 14476 Potsdam (Germany)

© 2023 The Authors. Angewandte Chemie International Edition published by Wiley-VCH GmbH. This is an open access article under the terms of the Creative Commons Attribution License, which permits use, distribution and reproduction in any medium, provided the original work is properly cited.

Introduction

Lanthipeptides constitute one of the most prominent compound families of the so-called ribosomally-synthesized and post-translationally modified peptides (RiPPs). The name lanthipeptide derives from the characteristic diamino diacid lanthionine involving the formation of various macrocyclic ring structures (Figure 1). To date, lanthipeptides have shown antibacterial,[1] antiviral,[2] morphogenic,[3] and antinociceptive[4] properties and thus have the potential as novel peptide therapeutics.[5]

Bacteria commonly encode the biosynthesis of lanthipeptides in biosynthetic gene clusters (BGCs). Main biosynthetic constituents are a lanthipeptide synthetase (Figure 1B) and a precursor peptide LanA. The latter consists of two segments: the N-terminal leader peptide (LP) is responsible for substrate recognition by its processing enzymes, while the C-terminal core peptide (CP) is modified and ultimately cleaved off from the LP to yield the mature lanthipeptide.[6]

The side-chain cross-links of lanthionine are introduced by lanthipeptide synthetases in a series of catalytic steps: i) site-specific activation of a Ser or Thr residue in the precursor peptide either by glutamylation[7] or phosphorylation,[8] ii) subsequent β-elimination yielding dehydroalanine (Dha) or dehydrobutyrine (Dhb), respectively, and iii) stereoselective Michael-type addition of an adjacent Cys thiol to the β-position of Dha or Dhb rendering the thioether-bridged macrocycle lanthionine (Lan) or methyllanthionine (MeLan), respectively (Figure 1A).[9]

The different biosynthetic principles and architecture of lanthionine synthetases are the basis for categorizing lanthipeptides into five classes (Figure 1B).[10] Class-I lanthipeptide synthetases utilize a glutamyl-tRNA-dependent enzyme called LanB[7] that activates and dehydrates the side chain of Ser/Thr through a glutamylation and β-elimination sequence. Subsequently, the cyclase LanC installs the thioether ring by activating a cysteine thiol using Zn^{II} as a cofactor.[7,11] Class-II enzymes (LanM) consist of two catalytic domains, namely a bifunctional dehydratase domain that dehydrates Ser/Thr through phosphorylation and elimination in a highly concerted fashion and a LanC-like cyclase domain for thioether formation.[12] The tri-domain synthe-

 © 2023 The Authors. Angewandte Chemie International Edition published by Wiley-VCH GmbH

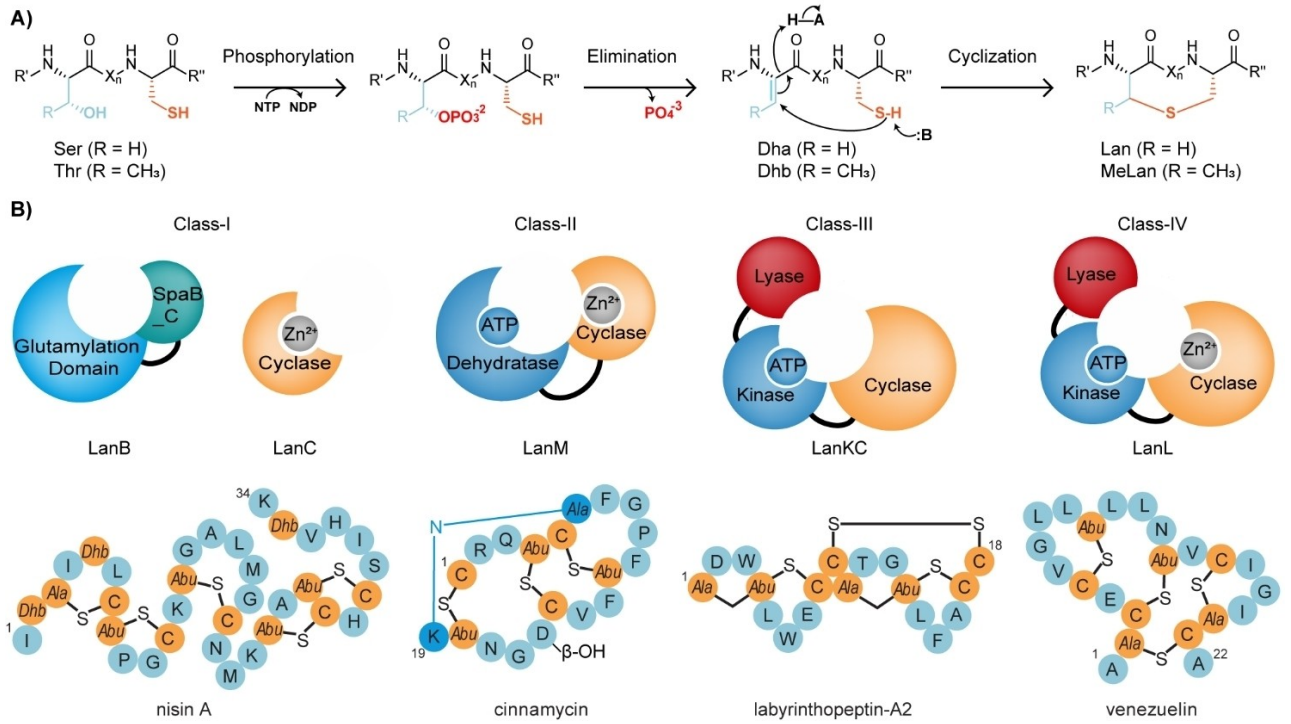

Figure 1. Lanthipeptide biosynthesis. A) Sequence of the catalytic steps of lanthionine macrocycle formation in classes II–IV. B) Domain organization of lanthipeptide synthetases from classes I–IV (top) and representative products (bottom). Class-V is not depicted in the Figure.

tases of class III (LanKC) and IV (LanL) assign each catalytic step to one specialized domain and thus comprise a kinase (phosphorylation), lyase (elimination), and cyclase domain (thioether formation).[13] Whilst class-IV enzymes, similar to classes I and II, have been reported to require Zn^{II} as a cofactor, cyclase domains of class III appear to employ a Zn^{II}-independent mechanism.[13] There have been only four class-IV lanthipeptides characterized to date: venezuelin (Figure 1B),[14] streptocollin,[15] globisporin[16] and SflA.[17] Class-V lanthipeptide synthetases catalyze the same reaction steps as classes III and IV, but they are carried out by individual enzymes, namely by kinase LanK, lyase LanY,[10b] and cyclase LanC.[18]

Within their respective clades, LPs of lanthipeptides are highly conserved, and accordingly RiPP enzymes harbor conserved regions for LP recognition. For instance, the RiPP recognition element (RRE)[19] was identified as LP-binding platform for several RiPP systems, however, in lanthipeptide synthetases this motif was only observed in class I.[19] For class-II synthetase HalM2, experiments indicated that the LP would bind to its capping-helices in the dehydratase domain.[20] The highly homologous class-III and -IV lanthipeptide synthetases have been proposed to use their kinase domain to bind the LP.[16,19] While RiPP biosynthesis is varied, hydrophobic interactions appear to play an important role in molecular recognition of LPs.[7,21] Analysis of LP sequences suggests short hydrophobic packing motifs to be critical for LP recruitment.[10b,20–22] For example, LPs of class-I, -II and -III lanthipeptides have been reported to display α-helical character in solution.[20,23] However, in the case of the class-I lanthipeptide nisin, the LP of NisA adopted β-strand conformation when bound to the RRE of NisB. To date, there are no structures of class-II to -V lanthipeptide synthetases bound to their cognate LPs available. The lack of structural information on class-III and -IV synthetases currently limits a mechanistic understanding of substrate recruitment, enzymatic processing, and lanthipeptide engineering.[24]

This work presents a new clade of class-IV lanthipeptides, with the first member discovered from *Thermomonospora curvata* DSM43183 (*T. curvata*). Moreover, we obtained the first crystal structure of a full-length class-IV synthetase at 2.7 Å resolution. The circular domain arrangement of CuvL renders a central substrate chamber and minimizes the distance between the three catalytic centers for efficient substrate translocation and multi-step processing. We ultimately demonstrate that the peptide substrate is recruited to the kinase domain at the lyase-kinase interface by means of an amphipathic α-helix in its LP region.

Results and Discussion

Curvocidin is a tricyclic lanthipeptide

The lanthipeptide curvocidin was identified from *T. curvata*, a thermophilic bacterium of the Actinobacteria phylum.[25] We performed genome mining of *T. curvata* using BAGEL[26] and found that the strain harbors an unknown class-IV lanthipeptide BGC (Figure 2A & Figure S1), which

© 2023 The Authors. Angewandte Chemie International Edition published by Wiley-VCH GmbH

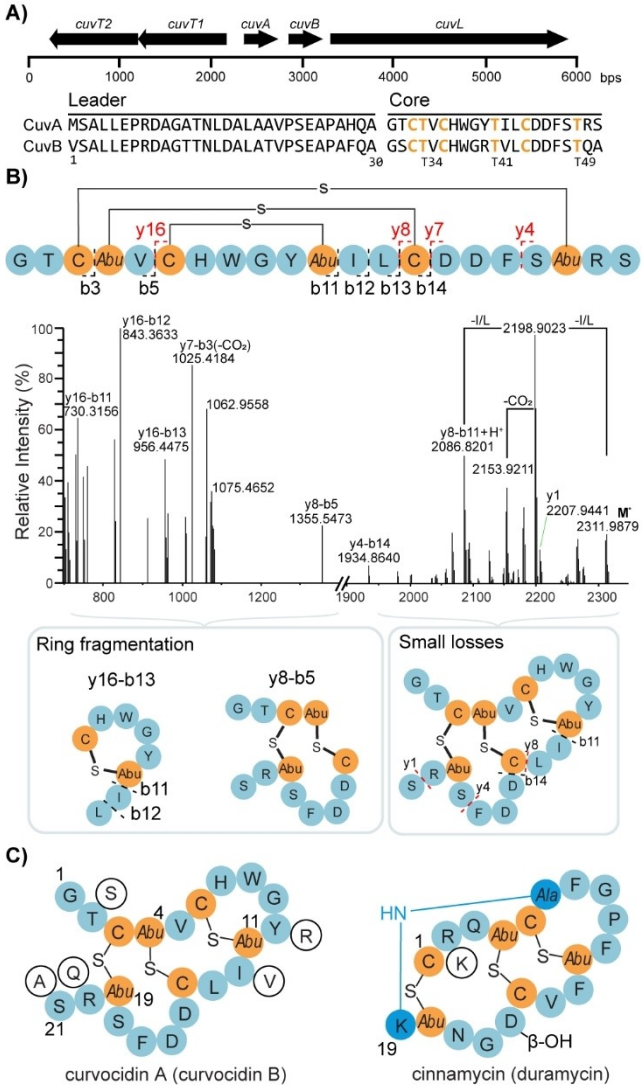

Figure 2. Structure of curvocidin A. A) Schematic of the *cuv* BGC and alignment of its precursor peptides CuvA and CuvB. LP/CP regions are indicated. Relevant Thr/Cys residues are highlighted in orange. B) Structure elucidation of curvocidin A by MS^2 fragmentation and assignment of fragments in the linear schematic of the peptide with annotated b- (black lines) and y-ions (red lines) (above spectrum) and ring patterns. For clarity, only relevant regions of the deconvoluted spectrum are shown (full spectrum in Figure S4). Abu refers to aminobutyric acid. C) Ball representation of curvocidin A with variations of curvocidin B in line balls (left). The scaffold of cinnamycin (line ball for duramycin) shows topological similarities (right).

we named the *cuv* cluster. The five genes of the cluster were assigned to encode for two precursor peptides (CuvA/CuvB), a modifying enzyme (CuvL), and two transporter proteins (CuvT1/T2).

We were able to detect curvocidin A by HPLC-ESI mass spectrometry (MS) when *T. curvata* was triggered by the stressor vanadium(V)-oxide[27] (Figure S2). Due to very low titers, the subsequent characterization of curvocidin was established by heterologous expression of the *cuv* cluster in *S. coelicolor* A3(2) M145 (see Experimental Procedures). This approach yielded the three peptide variants curvocidin A_{Gly}, curvocidin A_{Ala}, and curvocidin A_{Gln} which correspond to curvocidin A with different N-terminal extensions (Table S1 and Figure S3). Interestingly, we could not detect curvocidin B in neither strain. ESI-MS/MS experiments showed that parent curvocidin A from *T. curvata* corresponded to curvocidin A_{Gly} in *S. coelicolor* (Figures S2 and S3). The variable N-terminus of heterologous products likely was a result of the less specific processing by aminopeptidases[28] in *S. coelicolor*.

The MS assignment revealed that the observed molecular masses of 2510.1006 Da (curvocidin A_{Gln}), 2382.0318 Da (curvocidin A_{Ala}), and 2310.9987 Da (curvocidin A_{Gly}) formally corresponded to cleaved CuvA with three dehydrations (Table S1). Furthermore, MS/MS fragmentation confirmed the presence of three thioether bridges and established their connectivity (Figure 2B and Figure S4). Only internal fragments and the fragment of the innermost ring (y16-b11: 730.3156 Da, y16-b12: 843.3633 Da and y16-b13: 956.4475 Da) with a cross-link between Cys6 and Dhb11 were detected (Figure 2B, ring fragmentation). There was no y-ion matching fragmentation of the C-terminus, eliminating the possibility of Cys14-Dhb19 cross-links (Figure 2C). Thus, Cys3 is cross-linked with Dhb19, which was further corroborated by our in vitro assays (see below). Hence, curvocidin A is a tricyclic lanthipeptide which adopts a zipper-like topology similar to that of cinnamycin[29] or duramycin[30] (Figure 2C). We could not detect any antimicrobial activity for curvocidin A (Table S2), hence the biological activity of class-IV lanthipeptides remains unknown.

CuvL adopts a circular domain arrangement

The lanthipeptide synthetase CuvL was heterologously produced in *E. coli*. Purified CuvL (see Experimental Procedures and Figure S5) demonstrated high thermostability with a melting temperature T_m of $62.6 \pm 0.3\,^{\circ}C$ (Figure S6). The precursor peptide CuvA and its variants, as well as the leader peptide $CuvA_{LP}$ were obtained from heterologous production in *E. coli* or solid-phase peptide synthesis (SPPS) followed by preparative HPLC in high purity (see Experimental Procedures, Tables S3 and S4). We established an in vitro activity assay to monitor CuvA modification by wild-type CuvL and selected variants thereof (end-point determination, see Experimental Procedures). In ESI-MS measurements, CuvA ionized to a $[M+5H]^{5+}$ species, in which a single dehydration event for CuvA renders a mass shift of m/z −3.6 ($-H_2O$) and modification of a free thiol by iodoacetamide (IAM) yields a shift by m/z +11.4 (+AM). The assay showed that purified CuvL was catalytically active and installed the three native thioether bridges into CuvA (Figure S7). Moreover, by employing Thr-to-Ala variants of CuvA we managed to decipher the potential order of cyclization steps, with the first MeLan bridge being installed between Dhb34 and Cys44 (I, "central"), followed by bridges Cys33-Dhb49 (II, "outer") and finally Cys36-Dhb41 (III, "inner thioether") (Figure S8–S10).

© 2023 The Authors. Angewandte Chemie International Edition published by Wiley-VCH GmbH

We then set up crystallization trials with CuvL in the absence and presence of $CuvA_{LP}$ as well as with the non-hydrolysable adenosine-triphosphate (ATP) analog, adenylyl-imidodiphosphate (AMP-PNP). Two diffraction data sets were obtained. The first data set of seleno-methionine (SeMet)-labelled CuvL (PDB entry: 8CAR) was used for single anomalous dispersion (SAD)-phasing and the structure was refined at 2.7 Å resolution (R_{work}/R_{free} values of 0.301/0.336, Figure S11, Table S5). This data set was devoid of electron density for $CuvA_{LP}$ and AMP-PNP, despite their molar excess during crystallization. Subsequent trials were made using CuvL with a C-terminal strep-II tag for stability/purification purposes. The corresponding data set (PDB entry: 8CAV) was refined to a resolution of 2.9 Å (R_{work}/R_{free} values of 0.237/0.293, Figure 3, Table S5). Importantly, the second data set showed electron density for both AMP-PNP and $CuvA_{LP}$ in both molecules of the asymmetric unit (Figure S12). However, we did not model side-chains of $CuvA_{LP}$ since electron density was not sufficiently defined indicating dynamics.

The CuvL structures revealed an overall circular organization of its three catalytic domains (Figure 3). The N-terminal lyase domain employs a unique structural motif of two opposing β-hairpins that dock into a groove in the C-terminal cyclase domain, thereby closing the circular domain arrangement. To the best of our knowledge, this super-secondary structural motif has not been described before. Given its characteristic topology (Figure 3), we coined it a β-bow tie (see below). The lyase-cyclase domain closure establishes a central chamber of approximately 15–20 Å diameter that provides access to all three catalytic sites with mutual distances in the range of 30–38 Å. We consider this specific domain arrangement essential for iterative modification of substrate peptides. All domains and their features are described individually in the following subchapters.

The kinase domain recruits the leader peptide

The catalytic pathway of lanthipeptide maturation is initiated by the phosphorylation reaction. The responsible kinase domain comprises an N-terminal (N-lobe) and a C-terminal (C-lobe) subdomain, which harbor an interjacent nucleotide binding cleft (Figure 4A). The N-lobe consists of an α-helix that packs from one side onto a five-stranded antiparallel β-sheet. It is the N-lobe which represents the major interface to the neighboring lyase domain (Figure 3). In our initial SeMet-CuvL model, we were not able to model all amino acids owing to a substantial lack of electron density, in particular for residues Ser203-Ile297 of the kinase N-lobe (Figure S11). The poor electron density at this domain interface suggested structural flexibility, potentially modulated by the presence of $CuvA_{LP}$. By contrast, the second data set allowed us to also model the kinase N-lobe as well as the preceding 40-residue interdomain linker (gate loop) that connects the N-lobe with the β-bow tie of the lyase domain.

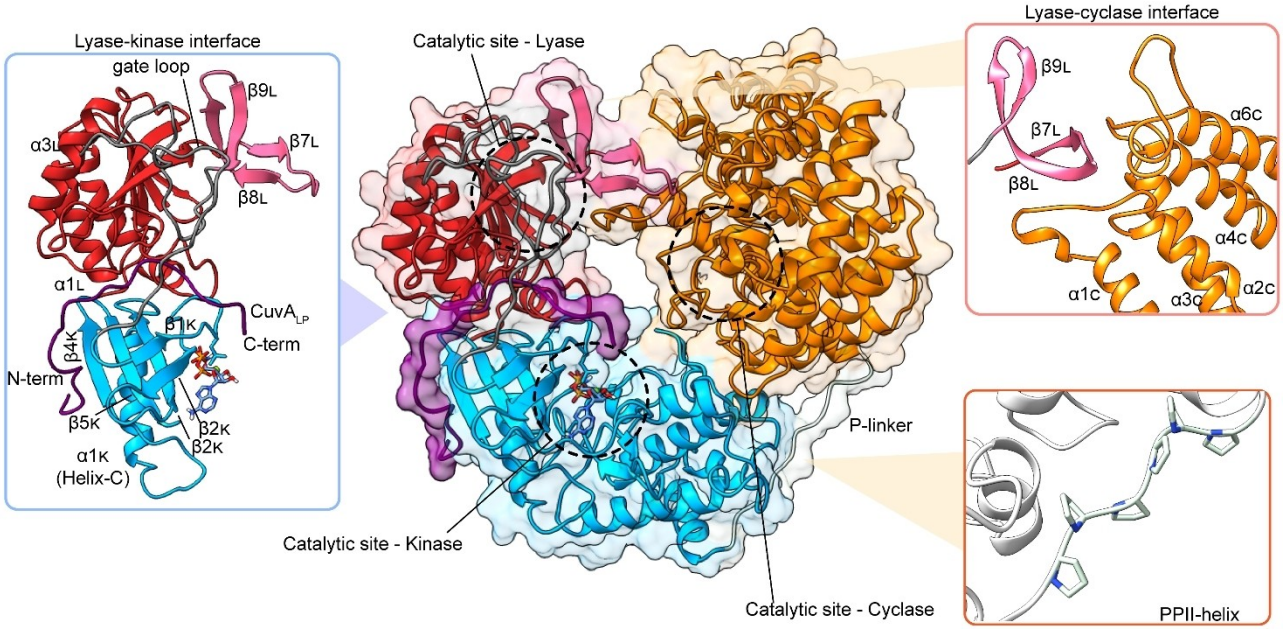

Figure 3. Overall fold of CuvL. Surface model of CuvL (PDB: 8CAV) with the lyase (red), kinase (blue), and cyclase (orange) domains forming a circular arrangement, which is achieved by docking the β-bow tie (pink - strands $\beta7_L$-$\beta9_L$) from the N-terminal lyase domain into the C-groove of the C-terminal cyclase domain. The backbone trace of $CuvA_{LP}$ is illustrated in purple. $CuvA_{LP}$ binds to the N-lobe of the kinase domain, threading through the gate loop (gray) that connects the β-bow tie of the lyase domain with the N-lobe of the kinase domain. The N-terminus of $CuvA_{LP}$ is assumed to be located on the outer surface of CuvL to supply the C-terminal CP substrate into the inner reaction chamber. Domain-domain interfaces are depicted in cartoon mode in the insets. Relevant secondary structure elements are labeled (extensions L, K, and C indicate lyase, kinase, and cyclase domains, respectively). Dashed circles highlight catalytic centers. AMP-PNP is depicted in stick mode.

© 2023 The Authors. Angewandte Chemie International Edition published by Wiley-VCH GmbH

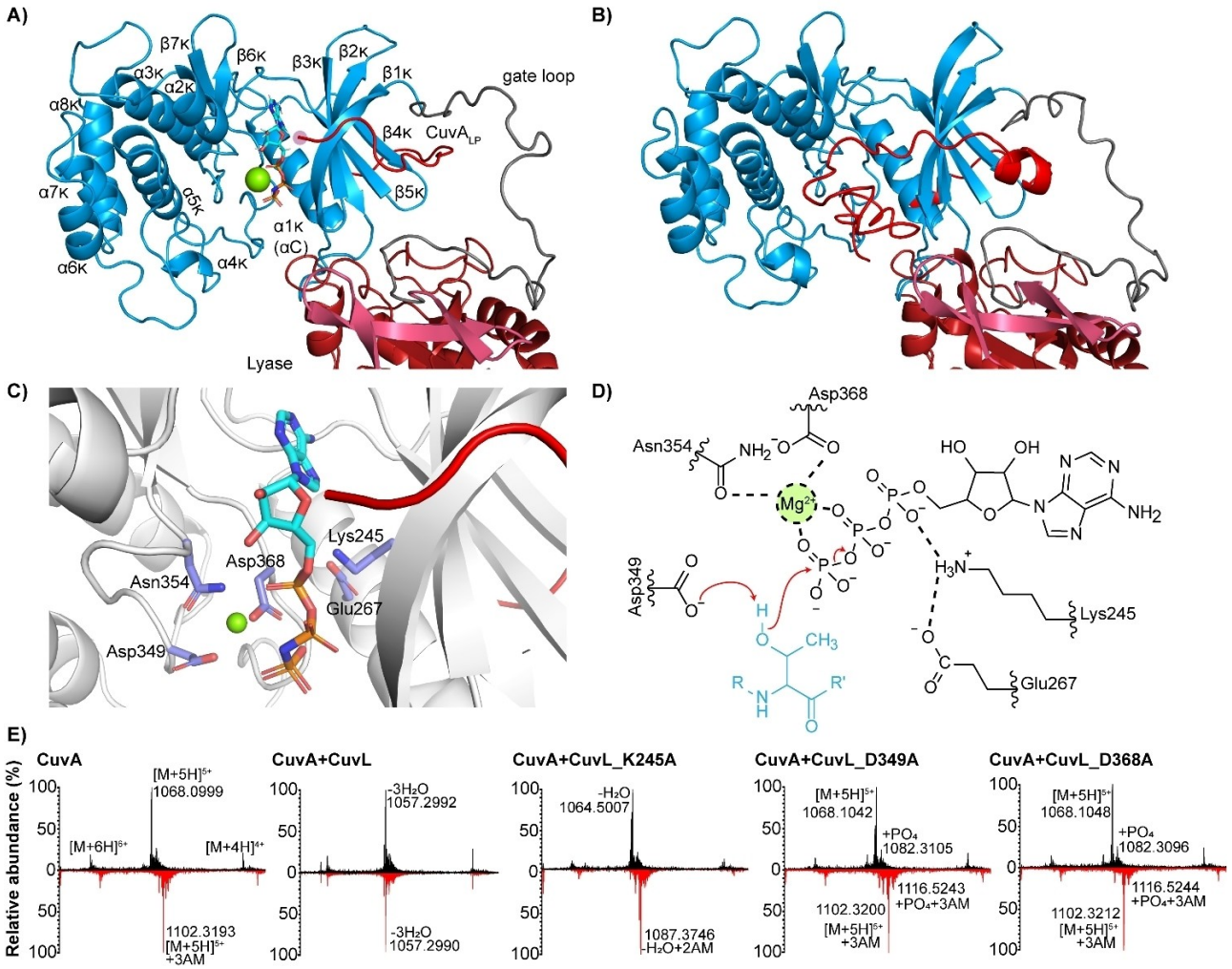

Figure 4. The kinase domain of CuvL. A) N- and C-lobes of the kinase domain (blue) with bound $CuvA_{LP}$ (red). The C-terminus (red circle) of $CuvA_{LP}$ is facing into the catalytic chamber of CuvL. The lyase domain is displayed in dark red. B) AlphaFold2-model of the kinase domain (blue) bound to CuvA (red). C) Catalytic center with bound AMP-PNP and Mg^{2+} (green sphere). D) Scheme of the proposed phosphorylation mechanism. The Thr substrate is drawn in light blue. E) ESI-MS spectra of in vitro assays for dehydration (black) and IAM labeling (red) of CuvA in the absence/presence of CuvL and its variants.

Based on the crystal structure and homologous kinase sequences (Figure S13), residues Asn354 ($L8_K$) and Asp368 (DFG motif in $L10_K$) are responsible for coordination of Mg^{2+} for ATP activation (Figure 4C). The phosphate transfer could be mediated by residue Asp349 (HRD motif located on $L8_K$), acting as a catalytic base to abstract the hydroxyl proton from the Thr substrate (Figure 4D).[31] Lys245 comes into contact with Glu267 in $\alpha1_K$, the α-phosphate and the ribose subunit of ATP (Figure 4A) and is thus likely involved in ATP/substrate sensing.[6,32] Substitutions in the active site, e.g. in CuvL_D349A and CuvL_D368A, virtually abolished phosphorylation activity in our in vitro assay (Figure 4E). The variant CuvL_K245A managed to perform only one dehydration and cyclization. The assays thus showed that conserved residues Lys245, Asp349, and Asp368 play an important role for the kinase activity of CuvL (Figure S13).

During model building with the second dataset (PDB entry: 8CAV), we observed additional electron density not originating from CuvL but stretching across the surface of the N-lobe from the outward helix $\alpha1_K$ and threading through the gate loop towards the inner chamber of CuvL (Figures 4, 5 and Figure S14). We anticipated this density to arise from $CuvA_{LP}$ but could only model a peptide backbone into the density leaving specific side-chain contacts in the LP binding site undetermined. Intriguingly, an artificial intelligence (AI)-based model of the CuvL-CuvA complex using AlphaFold2 and AlphaFold-multimer[33] (Figure 4B, see Figure S15 and S16 for confidence scores of models) predicted that $CuvA_{LP}$ similarly wraps around the N-lobe of the kinase domain and threads through the gate loop (Figure 4B and Figure S14). In this model, the N-terminal residues Glu6 and Asp9 of $CuvA_{LP}$ interacted with the positively-charged surface residues of helix $\alpha1_K$ and strand $\beta4_K$, e.g. Arg265 and Arg288 (Figure 4A and 5). It should be noted that most LP

© 2023 The Authors. Angewandte Chemie International Edition published by Wiley-VCH GmbH

sequences of classes III and IV are of acidic character, whereas the complementary N-lobes bear basic surface residues (Figure 5, Figure S13 and S14). Furthermore, the LP backbone wraps around the N-lobe embedding several aliphatic side chains into hydrophobic pockets of the N-lobe and C-terminal residues of the gate loop (Figure 5). Importantly, bound $CuvA_{LP}$ adopted an amphipathic α-helix (Leu15-Val21) in the AI model with residues Leu15, Leu18 and Val21 lining its interacting face (Figure 5B). For class-III lanthipeptide MicA, we have previously shown that the unbound LP partially adopts an amphipathic α-helix in solution, which guides complex formation between substrate and synthetase.[23] A highly conserved $\theta_1xx\theta_2xx\theta_3$ motif (with θ representing a hydrophobic, mostly branched amino acid) was proposed to play a key role in LP recognition. We observed a similar α-helical propensity of $CuvA_{LP}$ by means of nuclear magnetic resonance (NMR) spectroscopy. The low signal dispersion in the ^1H dimension of ^1H-^1H TOCSY and ^1H-^{15}N HMQC spectra indicated that a major fraction of the peptide populated random-coil states (Figure S17).

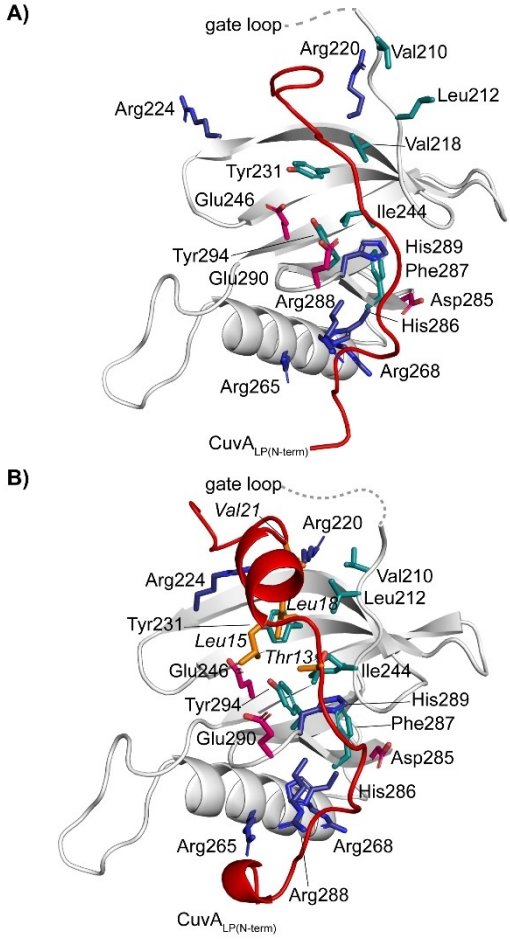

Figure 5. Leader peptide recruitment by the kinase domain of CuvL. A) Experimental structure of the kinase N-lobe (blue) with side chains interacting with $CuvA_{LP}$ (red). B) Corresponding AlphaFold2 model of CuvL and $CuvA_{LP}$ (residues in italics). Interacting residues are depicted in stick mode and colored: hydrophobic (cyan), negatively-charged (pink) and positively-charged (dark blue).

However, characteristic NOE patterns as well as secondary chemical shifts pointed to an α-helical propensity of $CuvA_{LP}$ in the region Ala12 to Ala19 (Figure S18–S20, Tables S6 and S7), which virtually covers the interacting α-helix in the AlphaFold2 model.

To further support the LP binding mode, we generated AI models for other lanthipeptide systems, e.g. the class-III MicKC-MicA (microvionin) or the class-IV VenL-VenA (venezuelin) complexes (Figure S21, see Figures S15 and S16 for confidence scores of models). All models consistently positioned the LP on the N-lobe β-sheet of their respective synthetase and oriented the C-terminal CP towards the central reaction chamber. In agreement with our previous study,[23] MicA adopted an amphipathic α-helix in this model, with Leu3 (θ_1), Leu6 (θ_2) and Leu9 (θ_3) being packed onto the mostly hydrophobic face of the N-lobe β-sheet (Figure S21). Due to its shorter sequence, $MicA_{LP}$ could not pass the gate loop to wrap around the N-lobe. As such we observe that some LPs, e.g. CuvA and SflA possess an N-terminal extension acting as a hook-like element that interacts with helix $\alpha1_K$ on the outer surface of LanL/LanKCs (Figure 5 and Figure S21). Interestingly, in the AI model of the standalone kinase LmxK (class-V),[34] the hydrophobic β-sheet face of the N-lobe was covered with its own N-terminal α-helix in a similar mode to that of LPs (Figure S21).

The structure of the excised kinase domain of the class-III synthetase CurKC from *T. curvata* bound to adenosine has been recently reported.[21a] The authors proposed the N-lobe as a major LP binding region of CurKC and indicated that native lyase-kinase domain contacts are required to recruit the LP efficiently. However, their molecular dynamics (MD) simulations predicted an LP binding site that we consider as inaccessible and too close to the ATP binding site. Importantly, the AlphaFold-multimer model of CurKC-CurA was consistent with all other AI models and our experimental data on CuvL-CuvA (Figure S21).

Our findings thus provide the structural basis for LP recruitment in class-III and -IV lanthipeptide synthetases. We conclude that class-III and -IV LPs exhibit α-helical propensities (Figure S22 and S23), which may become triggered or modulated by interaction with the kinase N-lobe of LanKC and LanL enzymes, respectively. Our modeling approaches using AlphaFold2 suggest coevolution of residues in the α-helical region of LanA and the kinase N-lobe of LanL/LanKC, thus allowing to define a leader recognition code for classes III and IV (Figure S23).

Finally, the C-lobe of the kinase domain consists of six α-helices and two β-strands (Figure S24). Helices $\alpha2_K$, $\alpha4_K$, $\alpha5_K$ and the interjacent loops are deployed to settle on the C-terminal cyclase domain. The largest difference to the structure of the excised CurKC kinase domain[21a] is the reorganization of α-helices $\alpha5_K$-$\alpha7_K$ including their outward translation to form the interface with the cyclase domain. The latter is connected to the C-lobe by a proline-rich linker (P-linker, Pro475-Pro480) adopting a polyproline helix II (PPII) conformation (Figure 3). The PPII is frequently found in intrinsically disordered proteins or protein regions, e.g. in interdomain linker regions at the edge of α-helices.[35]

© 2023 The Authors. Angewandte Chemie International Edition published by Wiley-VCH GmbH

Hence, structural plasticity at the kinase-cyclase interface might allow for domain movements during substrate conversion.

The phosphothreonine lyase domain of CuvL

The second reaction step of lanthipeptide biosynthesis is the β-elimination of phospho-Ser/Thr yielding Dha/Dhb residues (Figure 1). The responsible lyase domain of CuvL shows homology to other microbial phospho-Ser/Thr lyases such as SpvC[36] or OspF[37] but has evolved a unique structural feature. The above-mentioned β-bow tie (Pro153-Pro176) comprises strands $\beta7_L$ to $\beta9_L$ that form a twisted antiparallel β-sheet (Figure 6A). The central, elongated strand $\beta8_L$ connects the two opposing type-I β-turns (residues NDDG and DPQG, respectively). The two wings of the β-bow tie and the entrance/exit chains virtually form a triangle with the β-turns spanning an angle of about 110°. The β-bow tie of the N-terminal lyase domain is docked onto the C-terminal cyclase domain. Loop $L11_L$ and the flanking strands $\beta7_L$ and $\beta8_L$ (N-terminal wing) are nested in the C-groove formed by the loops between helices $\alpha1_C/\alpha2_C$, $\alpha3_C/\alpha4_C$ and $\alpha5_C/\alpha6_C$ of the cyclase domain (Figure S25A–B). The C-groove mediates hydrophobic interactions on its bottom, while its rim is mostly decorated with polar and positively-charged residues attracting the acidic N-terminal wing of the β-bow tie. Corresponding acidic residues Asp159, Asp160 and Asp162 are located near the catalytic center of the cyclase domain, e.g. Asp160 is in 6 Å and 8 Å vicinity of His610 and Tyr525. Given the fact that strand $\beta9_L$ of the β-bow tie leads into the gate loop, we assume an allosteric network between the β-bow tie of the lyase domain, the C-groove of the cyclase domain and the N-lobe of the kinase domain, where the LP of the substrate is bound. To address the functional role of the β-bow tie, we deleted its region rich in Asp residues (CuvL_ΔD156-L163) thereby disrupting the β-bow tie structure itself. This variant was produced in very low amounts ($\approx 0.3\ mg\,L^{-1}$), whereas WT CuvL and other variants typically yielded 30–40 $mg\,L^{-1}$ of *E. coli* culture. In the in vitro assay, CuvL_ΔD156-L163 yielded lower amounts of cyclized CuvA compared to the WT enzyme (Figure 6D). These results indicate an important role of the β-bow tie for protein stability and catalytic conversion, which may explain why excised cyclase domains of class-III and -IV lanthipeptide synthetases have not been successfully obtained as soluble proteins.[16] Single Ala substitutions of the highly abundant Asp residues in the β-

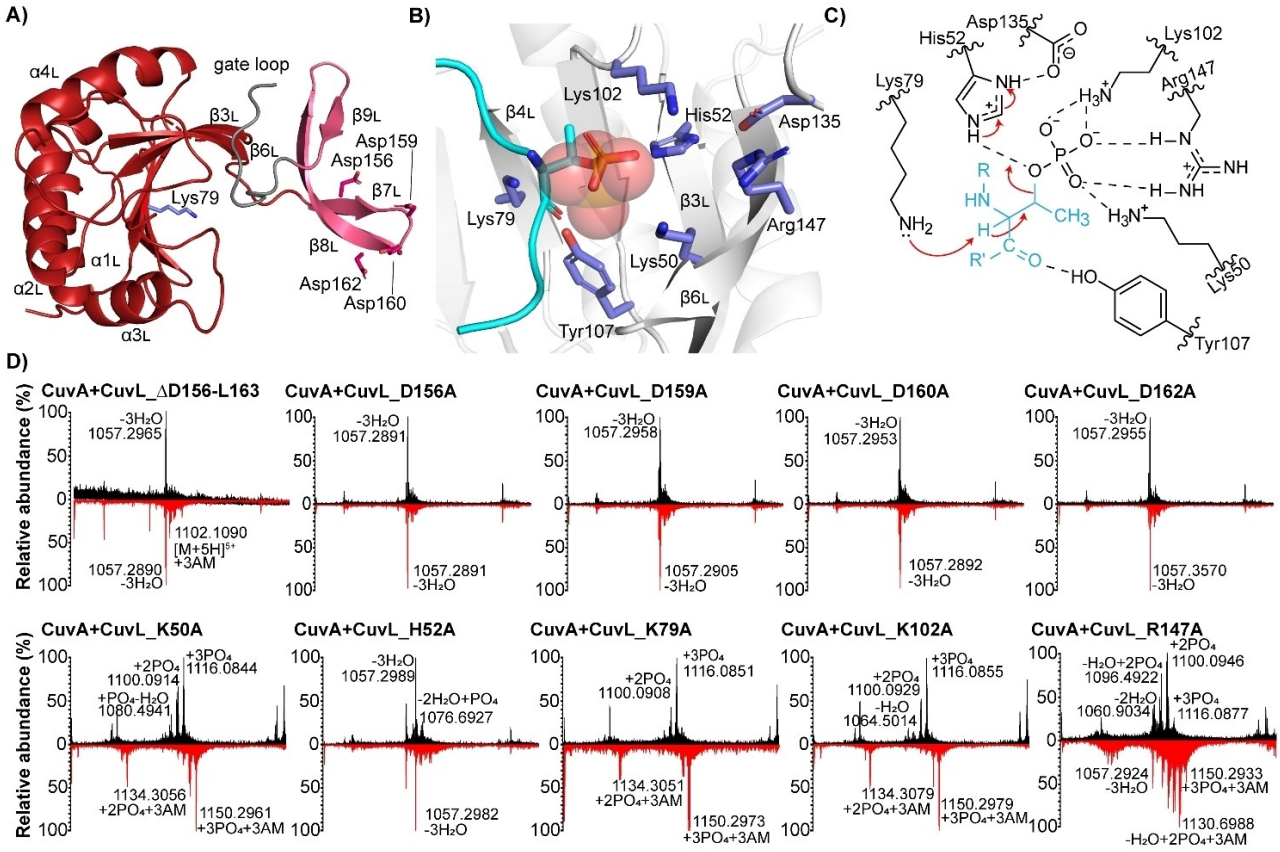

Figure 6. The lyase domain of CuvL. A) Lyase domain (dark red) with secondary structure elements labeled, and catalytic Lys79 shown in stick mode. The β-bow tie (pink) is followed by the gate loop (gray) extending towards the kinase domain. B) Catalytic center of the CuvL lyase domain (purple) with bound phosphate ion (transparent spheres) being superimposed with pThr substrate (cyan) from the co-crystal structure of SpvC (PDB: 2Z8P).[36] C) Proposed mechanism of β-elimination. D) ESI-MS spectra of in vitro assays for lyase variants in the β-bow tie (top row) and the catalytic center (bottom row). Dehydration and IAM labeling are shown in black and red respectively. Control reactions shown in Figure 4E.

© 2023 The Authors. Angewandte Chemie International Edition published by Wiley-VCH GmbH

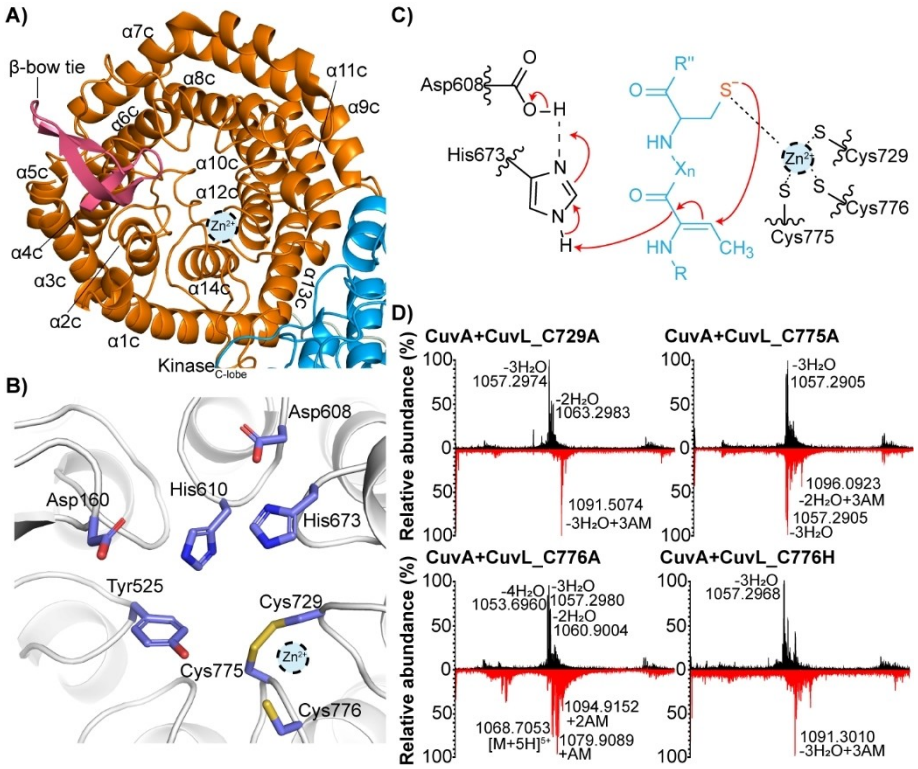

Figure 7. The cyclase domain of CuvL. A) Cyclase domain (orange) with secondary structure elements labeled. The β-bow tie of the lyase domain (pink) and the C-lobe of the kinase domain (blue) are shown for context. B) Catalytic center (purple sticks) with disulfide bridge between residues Cys729 and Cys775. The potential position of Zn^{II} (dashed sphere) was approximated by superimposing holo-NisC (PDB: 2G0D) onto the CuvL structure. C) Proposed mechanism of cyclization by class-IV lanthipeptide synthetases. D) ESI-MS spectra of in vitro assays for cyclase variants of CuvL, with dehydration and IAM labeling shown in black and red, respectively. Control reactions shown in Figure 4.

bow tie (CuvL_D156A, D159A, D160A, and D162A) were not sufficient to elicit different product profiles compared to WT CuvL (Figure 6D).

The β-bow tie appears to be a conserved element in class-III and -IV lanthipeptide synthetases, which is corroborated by AI models of representative enzymes (Figure S25C). A similar β-hairpin topology is present in the cyclase domain of class-II synthetase CylM (residues Ala665-Ile689), where it is inserted between α-helices of the α/α-toroid fold.[12] Although differently arranged, the motif in CylM is a major interface between its dehydratase and cyclase domains, similar to the β-bow tie between the lyase and cyclase domains of CuvL (Figure S26). Hence, synthetases of class II, III, and IV may use the β-bow tie for docking and communication between the cyclase and its partner domains that deliver the dehydrated intermediates. Interestingly, AI models of the CuvL-CuvA complex indicated that the β-bow tie may also function as a sensor of reaction intermediates, as it was detached in some cases from the C-groove and instead directly involved in recognition of the substrate's CP region (Figure S27).

The catalytic center of the lyase domain shares high sequence identity to that of phosphothreonine lyase SpvC from *Salmonella enterica.* Superposition of the substrate from the SpvC crystal structure[36] (PDB entry: 2Z8P) to the lyase domain of CuvL allowed to assign mechanistic functions (Figure 6A–C). The phosphate moiety of the phospho-Thr (pThr) substrate is most likely coordinated by positively-charged residues Lys50, Lys102, and Arg147. Notably, we observed a phosphate ion in our initial SeMet model in an equivalent position to that of pThr in the SpvC-substrate co-crystal structure (Figure 6B). The corresponding substitutions K50A, K102A and R147A reduced dehydration activity of CuvL in vitro and abolished or significantly impaired downstream cyclization (Figure 6D). According to previous studies on SpvC,[36] residue Lys79, which is invariable amongst classes III and IV, would function as catalytic base that deprotonates pThr at the α-position. Indeed, the K79A replacement in CuvL completely abolished β-elimination in vitro, thereby accumulating phosphorylated CuvA species (Figure 6D). Furthermore, we assumed that conserved residue His52, which is held in place by Asp135 (3.5 Å distance), may function as catalytic acid by protonating the leaving phosphate (Figure 6C and Figure S28). The corresponding H106N variant of SpvC was reported to be incompetent of β-elimination.[36] However, we observed full conversion of CuvA by CuvL_H52A (Figure 6D), possibly because the leaving phosphate group may abstract the proton from a nearby water molecule.

© 2023 The Authors. Angewandte Chemie International Edition published by Wiley-VCH GmbH

The cyclase domain of CuvL

Cyclase domains of lanthipeptide synthetases catalyze the nucleophilic attack of Cys thiols on Dha/Dhb residues yielding cyclic thioethers. The cyclase domain of CuvL adopts a characteristic α/α-toroid fold (Figure 7A) that is very similar to class-I cyclase NisC[11] and the class-II cyclase domain of CylM.[12] Similarly to these systems, class-IV synthetases have been classified as Zn^{II}-dependent enzymes. We could not observe a bound Zn^{II} ion at the expected coordination site comprising conserved residues Cys729, Cys775, and Cys776 (Figure S29). We ascribe this result to the competing formation of a disulfide bridge between residues Cys729 and Cys775 (Figure 7B) under the oxidizing conditions during protein crystallization. Inductively-coupled plasma optical emission spectroscopy (ICP-OES) of freshly-purified CuvL yielded a holo-protein fraction of only 39.3 % (Table S8). The presence of exogenous Zn^{II} and a reducing agent during protein purification increased the holo-fraction to 85.7 %. However, CuvL appears to be susceptible to Zn^{II}-unloading under oxidative conditions during the rather large time window of crystallization. Importantly, *T. curvata* is a thermophile, preferring temperatures of about 50 °C and it is difficult to assess how physiological conditions in *T. curvata* affect the stability of the Zn^{II} coordination sphere in CuvL.

A superposition of holo-NisC[11] and apo-CuvL allowed to locate Zn^{II} vicinal to the Cys triad of CuvL with hypothetical metal-sulfur distances in the range of 3.1–4.4 Å (Figure 7B). Site-directed mutagenesis revealed that Cys729 and Cys776 were essential for cyclization activity, whilst CuvL_C775A was still capable of cyclizing CuvA, albeit with reduced activity (Figure 7D). The proposed catalytic mechanism of CuvL is based on the structure and mechanism of NisC,[11] LanCL1[38] and studies on the cyclase domain of SgbL[39] (Figure 7C). Future investigations are needed to understand the unusual properties of class-IV cyclase domains and how they achieve to position two substrate residues (Dha/Dhb and Cys) for regioselective cross-linking.

Conclusion

Despite a plethora of studies on genome mining and structure elucidation of novel RiPPs, including lanthipeptides,[12] the structural biology of class-III and -IV lanthipeptide synthetases has remained widely elusive.[8] Inherent conformational heterogeneity needed for the iterative multi-step processing of peptides may account for the difficulties in accessing the molecular structures of these trifunctional enzymes. The herein presented structure of CuvL thus provides important and general insights into class-IV enzymes with implications for class-III systems as well. Although our diffraction data suffers from low resolution for the bound LP, it allows to unambiguously pinpoint the binding surface at the kinase N-lobe. AlphaFold-Multimer[33] proved to be very useful in predicting synthetase-peptide complexes and supported the N-lobe as the recruitment platform. Virtually all tested LanA systems utilized an amphipathic α-helix with the previously reported $\theta_1xx\theta_2xx\theta_3$ motif[34] to dock onto the N-lobe near the kinase-lyase interface. Our NMR data of free $CuvA_{LP}$ confirmed the α-helical propensity of this motif. Since class-III and -IV LPs vary in length, N-terminal extensions seem to adopt elongated α-helices or to wrap around the N-lobe. Hence, our study provides a universal recognition code for prediction of binding residues in uncharacterized LanL/LanKC-LanA pairs, as well as rational design of precursor peptides (Figure S23). It should be noted that LPs sample conformational ensembles in solution and possibly in the bound state complicating structural analysis. Such structural plasticity may facilitate substrate movements between catalytic sites. Previous studies on class-II enzymes have demonstrated that dynamic interface regions and allosteric communication play an important role during lanthipeptide biosynthesis.[40] The CuvL structure reveals a circular domain arrangement closed by the β-bow tie that anchors the N-terminal lyase domain at the entrance of the C-terminal cyclase domain. While this arrangement minimizes the distances between catalytic centers and most likely assures an efficient shuttling of substrate intermediates within the inner reaction chamber, the β-bow tie may even be involved in transient interactions with these states and thus partially function as a guide and sensor of substrate conversion. These new insights into domain-domain interfaces will facilitate future studies on protein dynamics and allosteric communication using e.g., H/D-exchange MS or NMR spectroscopy.

In conclusion, we present the first crystal structure of a full-length class-IV lanthipeptide synthetase along with a general leader recognition code that appears applicable to all class-III and class-IV lanthipeptide systems. Our findings thus provide new opportunities for engineering and research into lanthipeptides.

Acknowledgements

The project was funded by the Deutsche Forschungsgemeinschaft (DFG, German Research Foundation) under Germany's Excellence Strategy—EXC 2008-390540038 (UniSysCat), the research training group RTG 2473 "Bioactive Peptides", project number 392923329 (M.G., C.H.K., R.S.) and the Studienstiftung des deutschen Volkes (M.G.). We acknowledge access to beamlines of the BESSY II storage ring (Berlin) through the Joint Berlin MX-Laboratory sponsored by Helmholtz Zentrum Berlin für Materialien und Energie, Freie Universität Berlin, Humboldt-Universität zu Berlin, Max-Delbrück-Centrum, and the Leibniz-Institut für Molekulare Pharmakologie. We thank Dr. Melanie Gonsior for providing LicM2 for this study. Open Access funding enabled and organized by Projekt DEAL.

Conflict of Interest

The authors declare no conflict of interest.

© 2023 The Authors. Angewandte Chemie International Edition published by Wiley-VCH GmbH

Data Availability Statement

Coordinates and structure factor amplitudes are available at the Protein Data Bank (PDB), www.wwpdb.org, under accession numbers 8CAR for SeMet-CuvL and 8CAV for CuvL:AMP-PNP:$CuvA_{LP}$.

Keywords: Enzymes · Lanthipeptide Synthetase · Lanthipeptides · Protein Structures · RIPPs

[1] a) G. A. Hudson, D. A. Mitchell, *Curr. Opin. Microbiol.* **2018**, *45*, 61–69; b) V. Wiebach, A. Mainz, M.-A. J. Siegert, N. A. Jungmann, G. Lesquame, S. Tirat, A. Dreux-Zigha, J. Aszodi, D. Le Beller, R. D. Süssmuth, *Nat. Chem. Biol.* **2018**, *14*, 652–654.

[2] G. Férir, M. I. Petrova, G. Andrei, D. Huskens, B. Hoorelbeke, R. Snoeck, J. Vanderleyden, J. Balzarini, S. Bartoschek, M. Brönstrup, R. D. Süssmuth, D. Schols, *PLoS One* **2013**, *8*, e64010.

[3] S. Kodani, M. E. Hudson, M. C. Durrant, M. J. Buttner, J. R. Nodwell, J. M. Willey, *Proc. Natl. Acad. Sci. USA* **2004**, *101*, 11448–11453.

[4] K. Meindl, T. Schmiederer, K. Schneider, A. Reicke, D. Butz, S. Keller, H. Gühring, L. Vértesy, J. Wink, H. Hoffmann, M. Brönstrup, G. M. Sheldrick, R. D. Süssmuth, *Angew. Chem. Int. Ed.* **2010**, *49*, 1151–1154.

[5] T. Dang, R. D. Süssmuth, *Acc. Chem. Res.* **2017**, *50*, 1566–1576.

[6] L. M. Repka, J. R. Chekan, S. K. Nair, W. A. van der Donk, *Chem. Rev.* **2017**, *117*, 5457–5520.

[7] M. A. Ortega, Y. Hao, Q. Zhang, M. C. Walker, W. A. van der Donk, S. K. Nair, *Nature* **2015**, *517*, 509–512.

[8] a) J. D. Hegemann, R. D. Süssmuth, *RSC Chem. Biol.* **2020**, *1*, 110–127; b) Y. Goto, A. Ökesli, W. A. van der Donk, *Biochemistry* **2011**, *50*, 891–898.

[9] Q. Zhang, Y. Yu, J. E. Vélasquez, W. A. van der Donk, *Proc. Natl. Acad. Sci. USA* **2012**, *109*, 18361–18366.

[10] a) P. G. Arnison, M. J. Bibb, G. Bierbaum, A. A. Bowers, T. S. Bugni, G. Bulaj, J. A. Camarero, D. J. Campopiano, G. L. Challis, J. Clardy, P. D. Cotter, D. J. Craik, M. Dawson, E. Dittmann, S. Donadio, P. C. Dorrestein, K.-D. Entian, M. A. Fischbach, J. S. Garavelli, U. Göransson, C. W. Gruber, D. H. Haft, T. K. Hemscheidt, C. Hertweck, C. Hill, A. R. Horswill, M. Jaspars, W. L. Kelly, J. P. Klinman, O. P. Kuipers, A. J. Link, W. Liu, M. A. Marahiel, D. A. Mitchell, G. N. Moll, B. S. Moore, R. Müller, S. K. Nair, I. F. Nes, G. E. Norris, B. M. Olivera, H. Onaka, M. L. Patchett, J. Piel, M. J. T. Reaney, S. Rebuffat, R. P. Ross, H.-G. Sahl, E. W. Schmidt, M. E. Selsted, K. Severinov, B. Shen, K. Sivonen, L. Smith, T. Stein, R. D. Süssmuth, J. R. Tagg, G.-L. Tang, A. W. Truman, J. C. Vederas, C. T. Walsh, J. D. Walton, S. C. Wenzel, J. M. Willey, W. A. van der Donk, *Nat. Prod. Rep.* **2013**, *30*, 108–160; b) H. Liang, I. J. Lopez, M. Sánchez-Hidalgo, O. Genilloud, W. A. van der Donk, *ACS Chem. Biol.* **2022**, *17*, 2519–2527.

[11] B. Li, W. A. Van der Donk, *J. Biol. Chem.* **2007**, *282*, 21169–21175.

[12] S.-H. Dong, W. Tang, T. Lukk, Y. Yu, S. K. Nair, W. A. Van der Donk, *eLife* **2015**, *4*, e07607.

[13] B. Krawczyk, G. H. Völler, J. Völler, P. Ensle, R. D. Süssmuth, *ChemBioChem* **2012**, *13*, 2065–2071.

[14] Y. Goto, B. Li, J. Claesen, Y. Shi, M. J. Bibb, W. A. Van der Donk, *PLoS Biol.* **2010**, *8*, e1000339.

[15] D. Iftime, M. Jasyk, A. Kulik, J. F. Imhoff, E. Stegmann, W. Wohlleben, R. D. Süssmuth, T. Weber, *ChemBioChem* **2015**, *16*, 2615–2623.

[16] J. D. Hegemann, W. A. van der Donk, *J. Am. Chem. Soc.* **2018**, *140*, 5743–5754.

[17] H. Ren, C. Shi, I. R. Bothwell, W. A. van der Donk, H. Zhao, *ACS Chem. Biol.* **2020**, *15*, 1642–1649.

[18] Z.-F. Pei, L. Zhu, R. Sarksian, W. A. van der Donk, S. K. Nair, *J. Am. Chem. Soc.* **2022**, *144*, 17549–17557.

[19] B. J. Burkhart, G. A. Hudson, K. L. Dunbar, D. A. Mitchell, *Nat. Chem. Biol.* **2015**, *11*, 564–570.

[20] I. R. Rahman, J. Z. Acedo, X. R. Liu, L. Zhu, J. Arrington, M. L. Gross, W. A. van der Donk, *ACS Chem. Biol.* **2020**, *15*, 1473–1486.

[21] a) S. Huang, Y. Wang, C. Cai, X. Xiao, S. Liu, Y. Ma, X. Xie, Y. Liang, H. Chen, J. Zhu, J. D. Hegemann, H. Yao, W. Wei, H. Wang, *Angew. Chem. Int. Ed.* **2022**, *61*, e202211382; b) J. D. Hegemann, L. Shi, M. L. Gross, W. A. van der Donk, *ACS Chem. Biol.* **2019**, *14*, 1583–1592.

[22] J. R. Chekan, C. Ongpipattanakul, S. K. Nair, *Proc. Natl. Acad. Sci. USA* **2019**, *116*, 24049–24055.

[23] V. Wiebach, A. Mainz, R. Schnegotzki, M.-A. J. Siegert, M. Hügelland, N. Pliszka, R. D. Süssmuth, *Angew. Chem. Int. Ed.* **2020**, *59*, 16777–16785.

[24] a) B. Krawczyk, P. Ensle, W. M. Müller, R. D. Süssmuth, *J. Am. Chem. Soc.* **2012**, *134*, 9922–9925; b) W. M. Müller, T. Schmiederer, P. Ensle, R. D. Süssmuth, *Angew. Chem. Int. Ed.* **2010**, *49*, 2436–2440; c) N. A. Jungmann, B. Krawczyk, M. Tietzmann, P. Ensle, R. D. Süssmuth, *J. Am. Chem. Soc.* **2014**, *136*, 15222–15228.

[25] A. Henssen, *Arch. Mikrobiol.* **1957**, *26*, 373–414.

[26] A. J. van Heel, A. De Jong, C. Song, J. H. Viel, J. Kok, O. P. Kuipers, *Nucleic Acids Res.* **2018**, *46*, W278–W281.

[27] a) Y. Tanaka, T. Hosaka, K. Ochi, *J. Antibiot.* **2010**, *63*, 477–481; b) D. Rehder, *Metallomics* **2015**, *7*, 730–742.

[28] S. Chen, B. Xu, E. Chen, J. Wang, J. Lu, S. Donadio, H. Ge, H. Wang, *Proc. Natl. Acad. Sci. USA* **2019**, *116*, 2533–2538.

[29] D. A. Widdick, H. M. Dodd, P. Barraille, J. White, T. H. Stein, K. F. Chater, M. J. Gasson, M. J. Bibb, *Proc. Natl. Acad. Sci. USA* **2003**, *100*, 4316–4321.

[30] F. Hayashi, K. Nagashima, Y. Terui, Y. Kawamura, K. Matsumoto, H. Itazaki, *J. Antibiot.* **1990**, *43*, 1421–1430.

[31] D. Fabbro, S. W. Cowan-Jacob, H. Moebitz, *Br. J. Pharmacol.* **2015**, *172*, 2675–2700.

[32] H. S. Meharena, X. Fan, L. G. Ahuja, M. M. Keshwani, C. L. McClendon, A. M. Chen, J. A. Adams, S. S. Taylor, *PLoS Biol.* **2016**, *14*, e2000127.

[33] a) J. Jumper, R. Evans, A. Pritzel, T. Green, M. Figurnov, O. Ronneberger, K. Tunyasuvunakool, R. Bates, A. Žídek, A. Potapenko, A. Bridgland, C. Meyer, S. A. A. Kohl, A. J. Ballard, A. Cowie, B. Romera-Paredes, S. Nikolov, R. Jain, J. Adler, T. Back, S. Petersen, D. Reiman, E. Clancy, M. Zielinski, M. Steinegger, M. Pacholska, T. Berghammer, S. Bodenstein, D. Silver, O. Vinyals, A. W. Senior, K. Kavukcuoglu, P. Kohli, D. Hassabis, *Nature* **2021**, *596*, 583–589; b) R. Evans, M. O'Neill, A. Pritzel, N. Antropova, A. Senior, T. Green, A. Žídek, R. Bates, S. Blackwell, J. Yim, O. Ronneberger, S. Bodenstein, M. Zielinski, A. Bridgland, A. Potapenko, A. Cowie, K. Tunyasuvunakool, R. Jain, E. Clancy, P. Kohli, J. Jumper, D. Hassabis, *bioRxiv* **2021**, https://doi.org/10.1101/2021.10.04.463034 .

[34] M. Xu, F. Zhang, Z. Cheng, G. Bashiri, J. Wang, J. Hong, Y. Wang, L. Xu, X. Chen, S.-X. Huang, S. Lin, Z. Deng, M. Tao, *Angew. Chem. Int. Ed.* **2020**, *59*, 18029–18035.

[35] A. A. Adzhubei, M. J. E. Sternberg, A. A. Makarov, *J. Mol. Biol.* **2013**, *425*, 2100–2132.

[36] Y. Zhu, H. Li, C. Long, L. Hu, H. Xu, L. Liu, S. Chen, D.-C. Wang, F. Shao, *Mol. Cell* **2007**, *28*, 899–913.

[37] H. Li, H. Xu, Y. Zhou, J. Zhang, C. Long, S. Li, S. Chen, J.-M. Zhou, F. Shao, *Science* **2007**, *315*, 1000–1003.

© 2023 The Authors. Angewandte Chemie International Edition published by Wiley-VCH GmbH

[38] C. Ongpipattanakul, S. Liu, Y. Luo, S. K. Nair, W. A. van der Donk, *Proc. Natl. Acad. Sci. USA* **2023**, *120*, e2217523120.
[39] J. D. Hegemann, R. D. Süssmuth, *ChemBioChem* **2021**, *22*, 3169–3172.
[40] a) K. A. Uggowitzer, A. R. Q. Shao, Y. Habibi, Q. E. Zhang, C. J. Thibodeaux, *Biochemistry* **2022**, *61*, 2118–2130; b) Y. Habibi, N. W. Weerasinghe, K. A. Uggowitzer, C. J. Thibodeaux, *J. Am. Chem. Soc.* **2022**, *144*, 10230–10240.

Manuscript received: March 3, 2023
Accepted manuscript online: April 4, 2023
Version of record online: April 27, 2023

© 2023 The Authors. Angewandte Chemie International Edition published by Wiley-VCH GmbH